RSC Advances

PAPER

View Article Online
View Journal | View Issue



Cite this: *RSC Adv.*, 2025, **15**, 14217

# Enhanced immunoregulation in traumatic urethral stricture repair utilizing a glycyrrhizic acid-infused antiswelling biogel scaffold

Zhihuan Zheng,† Ziqiang Wu,† Chao Li, Lei Zhou, Weibin Hou, Wei Xiong * and Shuo Tan*

As a prevalent complication following urinary system trauma, urethral stricture is characterized by progressive fibrosis and luminal narrowing often leading to recurrent dysuria and impaired renal function. Current treatments including surgical interventions face challenges such as high recurrence rates and secondary stenosis. Hydrogel-based drug delivery systems offer therapeutic potential but are limited by material swelling under urinary flow and insufficient modulation of inflammatory microenvironments. This study introduces an innovative anti-swelling carrageenan biogel scaffold (Car/Ga) functionalized with glycyrrhizic acid (Ga), a dual anti-inflammatory and immunoregulatory phytochemical. The Car matrix ensures structural stability in biological fluids by resisting swelling-induced obstruction while Ga targets trauma-induced inflammatory cascades through M1 macrophage polarization mitigation to reduce fibrotic progression. *In vitro* and *in vivo* evaluations demonstrate that the Car/Ga system synergistically combines urine stability with immunomodulatory bioactivity, significantly reducing pro-inflammatory cytokine levels (iNOS) and promoting M2 macrophage polarization (Arg1). Histological analyses reveal attenuated collagen deposition and enhanced epithelial regeneration in urethral stricture models, highlighting its capacity to disrupt the inflammation–fibrosis cycle. By addressing both urine stability and immunological dysregulation, this dual-functional biogel represents a transformative strategy for precise urethral repair, demonstrating potential for clinical translation in urethral repair applications.

Received 25th March 2025
Accepted 22nd April 2025

DOI: 10.1039/d5ra02083b

rsc.li/rsc-advances



## 1. Introduction

Urethral stricture is a common secondary pathological change in the urinary system, often triggered by trauma, infection, or iatrogenic injury. Its pathological characteristics include urethral mucosal fibrosis and excessive proliferation of scar tissue.[1] Excessive inflammation caused by injuries ultimately leads to progressive fibrosis and stricture of the urethral lumen, resulting in symptomatic dysuria and potentially impairing renal function.[2] Current treatment methods include urethral dilation, endoscopic resection, and open reconstructive surgery. However, these methods often come with high recurrence rates and various complications, such as scar formation and re-stenosis.[3] In recent years, biomaterial-mediated local drug delivery systems have provided new insights into overcoming this challenge.[4] Among them, hydrogels have garnered attention due to their three-dimensional network structure, excellent biocompatibility, and versatile drug-loading capabilities.[5]

However, current research predominantly focuses on optimizing the drug-loading capabilities of hydrogels[6] while overlooking the critical impact of the distinct urethral hydrodynamic microenvironment on material performance.[7] Conventional hydrogel formulations (*e.g.*, gelatin-based systems) frequently exhibit undesirable swelling upon prolonged exposure to biological fluids, potentially inducing secondary urethral obstruction – a fundamental limitation hindering clinical translation.[8] Concurrently, emerging evidence confirms that transitional inflammatory responses within trauma microenvironments and M1 macrophage polarization constitute pivotal initiators of fibrotic cascades.[9] This dual challenge necessitates the development of innovative hydrogel platforms that simultaneously maintain structural stability under urinary flow conditions and demonstrate immunomodulatory functionality, representing a crucial breakthrough for achieving precision repair in urethral regeneration.

Carrageenan is a natural polysaccharide hydrocolloid extracted from marine red algae, typically appearing as an odorless and tasteless white to pale yellow powder.[10] This hydrophilic polymer demonstrates remarkable viscosity and stability, exhibiting complete solubility in hot water to form

*Department of Urology, The Third Xiangya Hospital of Central South University, Changsha, 410013, China. E-mail: xiongweixy3@csu.edu.cn; tanshuo@csu.edu.cn*

† These authors contributed equally to this paper.

viscous transparent solutions that subsequently gel at room temperature.[11] Our research revealed that carrageenan-based hydrogels possess exceptional anti-swelling capacity, maintaining structural integrity in urinary environments without significant fluid absorption. This unique property positions them as promising candidates for urethral tissue repair applications.

In this study, we innovatively incorporated glycyrrhizic acid (Ga), a bioactive compound with dual anti-inflammatory and immunomodulatory functions, into carrageenan hydrogel (Car) systems to enhance their therapeutic potential (Fig. 1a). This pioneering approach aims to develop a novel biomaterial solution characterized by excellent biocompatibility and enhanced efficacy in preventing trauma-induced urethral stricture formation. The core concept of this strategy lies in leveraging the pharmacological properties of glycyrrhizic acid to directly target damaged areas, achieving protection and repair of the affected regions through a non-invasive approach. Specifically, by uniformly dispersing glycyrrhizic acid within the carrageenan gel network structure, the resulting composite not only inherits the excellent anti-swelling properties of the carrageenan hydrogel. More importantly, it is endowed with additional biological functions—namely, actively participating in the healing process of damaged tissues, rather than merely existing as a physical barrier (Fig. 1b).

## 2. Materials and methods

### 2.1. Materials

Carrageenan and glycyrrhizic acid were purchased from Aladdin (China). Fetal bovine serum (FBS), Phosphate buffer saline (PBS), cell counting kit-8 (CCK-8), and Dulbecco's modified Eagle medium (DMEM) were purchased from were Gibco (USA). All other reagents were of analytical grade.

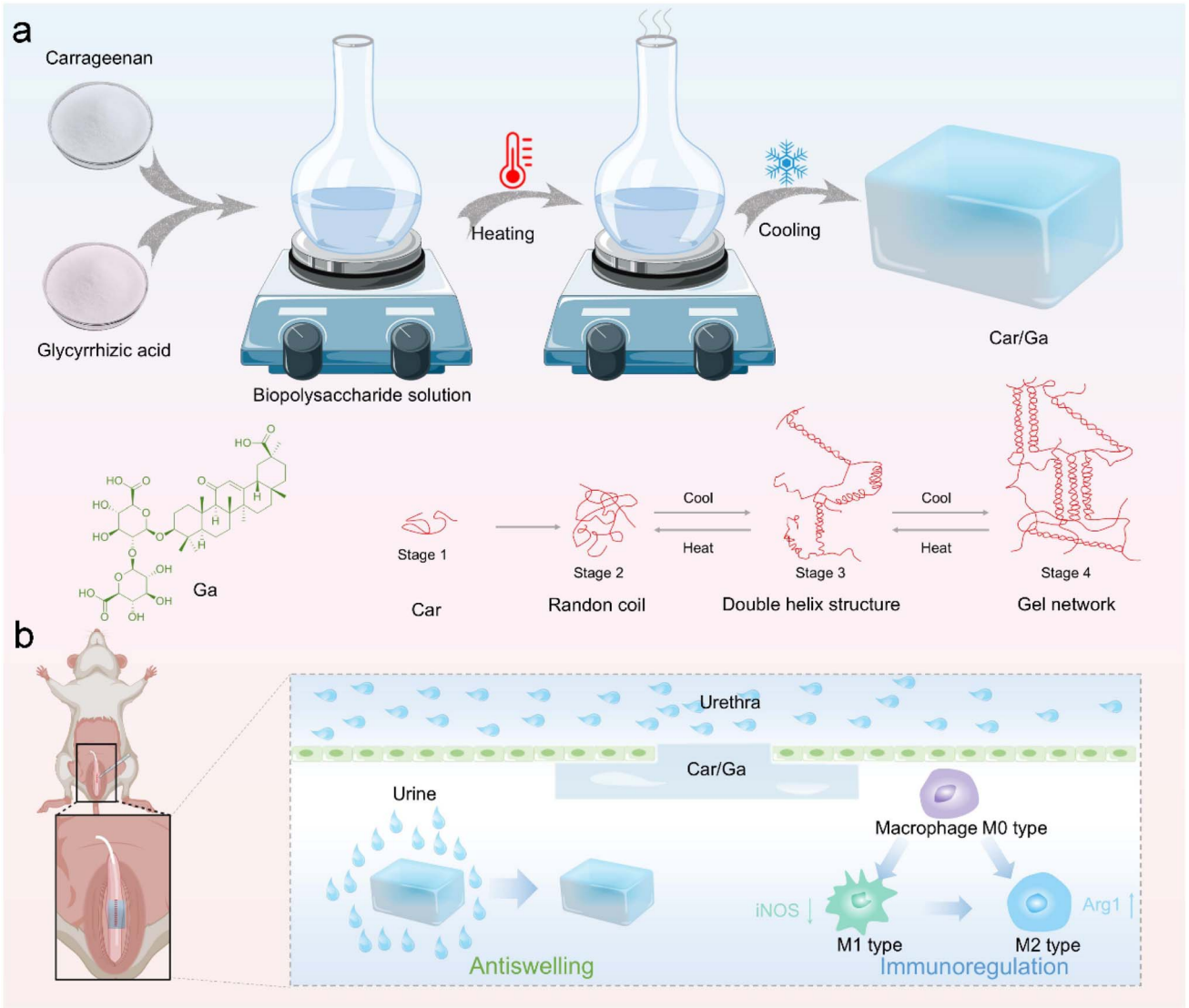


Fig. 1 (a) Schematic representation of the fabrication process for the Car/Ga hybrid hydrogel. (b) A schematic illustration of a multifunctional anti-swelling and immunomodulatory hydrogel for reconstructing traumatic urethral strictures.

### 2.2. Synthesis of Car/Ga biogel

Car solutions with concentrations of 5 wt% were prepared by dissolving Car powder in deionized water under continuous magnetic stirring at 95 °C until complete dissolution was achieved. During this process, 0.5 weight percent of Ga powder was incorporated. To compensate for water loss due to evaporation throughout the heating procedure, careful replenishment was carried out. Subsequently, the prepared Car solution was carefully transferred into pre-fabricated molds and left to naturally cool, solidifying into Car/Ga biogels.

### 2.3. Characterization of biogels

The Fourier transform infrared (FTIR) spectral characterization was performed on a Thermo Fisher Scientific Nicolet iS20 spectrometer, with measurements acquired across the mid-infrared region (4000–400 $cm^{-1}$) at 4 $cm^{-1}$ resolution. Complementary thermogravimetric analysis (TGA) was carried out using a PerkinElmer STA 6000 simultaneous thermal analyzer under nitrogen atmosphere (20 mL $min^{-1}$ flow rate) with a controlled heating regime of 10 °C $min^{-1}$ from ambient temperature to 600 °C.

### 2.4. Swelling test of biogel

This study employed a gravimetric method to investigate the anti-swelling properties of biogel in urine. The experimental protocol was as follows: pre-weighed biogel samples (denoted as $W_b$) were immersed in fresh urine samples. At predetermined time intervals, the specimens were retrieved from the urine and carefully blotted with moistened filter paper to remove excess surface liquid. The instantaneous weight ($W_t$) was then recorded. The swelling ratio (SR) of the biogel at various time points was calculated using the following equation:

$$SR = W_t/W_b \times 100\%$$

### 2.5. Compression test

For the compression testing, cylindrical biogel specimens measuring 20 mm in diameter and 40 mm in height were fabricated. Subsequently, various biogel samples were mounted on the testing platform of a universal testing machine (Instron 4202, Instron, USA) equipped with a 100 N load cell. Uniaxial compression tests were then conducted at a constant speed of 30 mm $min^{-1}$ under ambient conditions.

### 2.6. Blood compatibility test

In brief, 500 μL of rat blood was centrifuged at 3500 rpm for 5 minutes. The supernatant was carefully removed, and the pellet was thoroughly washed three times with PBS. The blood was then diluted to a final concentration of 5%. Subsequently, 250 mg of biogel sample was mixed with 750 μL of processed blood in test tubes. PBS and deionized water were designated as negative and positive controls, respectively. The tubes containing the mixed solutions were incubated at 37 °C with continuous shaking at 100 rpm for 60 minutes. Post-incubation, blood was centrifuged again at 3500 rpm for 5 minutes. Finally, the absorbance of the supernatant was measured at 545 nm using a microplate reader (Thermo Fisher Scientific Oy Ratastie 2, FI-01620 Vantaa, Finland). The percentage of hemolysis was calculated using the following equation: hemolysis (%) = [(sample absorbance – negative control absorbance)/(positive control absorbance – negative control absorbance)] × 100.

### 2.7. Cytocompatibility testing

Cytotoxicity evaluation of the biogel was performed using L929 mouse fibroblast cells with Live/Dead Cell Double Staining Kit and Cell Counting Kit-8 (CCK8). The experimental procedure was conducted as follows: L929 cells were initially seeded in 24-well plates containing DMEM culture medium and subsequently incubated at 37 °C in a 5% $CO_2$ atmosphere for 12 h. The biogel samples were then placed in Transwell inserts, with untreated group serving as the control. Following co-culturing the biogel with cells, cytotoxicity assessment was performed using the Live/Dead staining kit. Viable cells were labeled with Calcein AM (emitting green fluorescence), while dead cells were stained with propidium iodide (PI, emitting red fluorescence). To evaluate the proliferative status of L929 cells co-cultured with biogels, CCK8 assay was conducted. At 24 h and 72 h time points, the Transwell inserts were removed, followed by addition of CCK8 reagent and 1 h incubation. The cell viability was ultimately quantified by measuring the absorbance of CCK8 at 450 nm using a microplate reader.

### 2.8. Animal experiment

This study utilized male Sprague-Dawley (SD) rats (body weight 300 g) supplied by Slack Jingda Laboratory Animal Co., Ltd. (Hunan, China). The animals were housed in a strictly controlled specific pathogen-free (SPF) environment with a 12 hour light/dark cycle, receiving food and bedding replacement every 3–4 days. All experimental procedures were performed in compliance with institutional animal care guidelines and approved by the Animal Welfare Committee of Central South University, China (Approval No. 202112630). Twenty male SD rats were randomly assigned to three experimental groups: Control, Car, and Car/Ga groups. For infection prophylaxis, amoxicillin (50 mg $kg^{-1}$) was administered *via* intraperitoneal injection one hour prior to surgical procedures. Anesthesia was induced using isoflurane inhalation, followed by supine positioning of the animals.

Cystostomy procedure: (1) a midline abdominal incision was made to surgically expose the bladder. (2) A 1.0 mm diameter epidural catheter (Aoocn Medical, Changyuan, China) was inserted through a carefully created apical bladder incision. (3) The cystotomy site was closed using 5–0 absorbable polyglycolic acid (PGA) sutures. (4) The distal catheter segment was tunneled subcutaneously to the dorsal region for urinary drainage.

Urethral stricture modeling: (1) the penile urethra was exposed through a ventral skin incision. (2) A lubricated 0.03-inch polyurethane guidewire was inserted into the urethral lumen. (3) A 5 mm full-thickness incision was made in the

urethral wall under direct visualization of the guidewire. (4) The surgical site was treated with biogel followed by meticulous wound closure using fine sutures.

### 2.9. Histological evaluation

Retrograde urethrography was performed by administering contrast agent through a cystostomy catheter, enabling clear visualization of bladder and proximal urethral anatomy during urethral stricture evaluation. Simultaneously, distal urethral segments were assessed using contrast medium delivered *via* an epidural catheter. All contrast administration procedures were conducted by a single investigator. Evaluations were systematically performed at 4 weeks post-model establishment. Urethral tissue specimens were collected during the fourth postoperative week and immediately fixed in 4% paraformaldehyde solution for overnight preservation. Subsequent histological processing involved preparation of 4 μm-thick tissue sections for three analytical approaches: (1) morphological assessment using Hematoxylin and Eosin (H&E) staining; (2) collagen fiber distribution analysis *via* Masson's trichrome staining; (3) immunophenotypic characterization through immunofluorescence staining targeting iNOS and Arg1 markers.

### 2.10. Statistical analysis

Experimental data were presented as mean ± standard deviation (SD) derived from a minimum of three separate experiments. Statistical evaluations were performed using one-way ANOVA followed by Tukey's *post hoc* test through Origin 8.0 software. Significance thresholds were established as: NS (not significant) for $p > 0.05$, * for $p < 0.05$, ** for $p < 0.01$, and *** for $p < 0.001$.

## 3. Results and discussion

### 3.1. Synthesis and testing of car biogel

The carrageenan gelation process progresses through four distinct phases (Fig. 1a): (1) initial dissolution stage: carrageenan dissolves in hot water, with its molecules adopting irregular coil-like conformations (2) helical transition phase: as the temperature decreases to a critical threshold, these molecules undergo a structural transition to single helices. (3) Network formation stage: further cooling induces intermolecular interactions that stabilize double-helix formations, establishing a three-dimensional network structure accompanied by initial gelation phenomena. (4) Gel maturation phase: the final cooling stage promotes aggregation of these double helices into a consolidated gel matrix through intermolecular associations. The initial dissolution temperature was 95 °C. During the cooling phase, the temperature descent gradually slowed down. At the beginning, the cooling rate was approximately 20 °C $min^{-1}$, and at the end, it was about 5 °C $min^{-1}$, eventually decreasing to room temperature at 25 °C.

Fourier transform infrared (FTIR) spectroscopy was initially performed to investigate the chemical structure of Car/Ga (Fig. 2a). The results revealed characteristic O–H stretching vibrations at 3390 $cm^{-1}$ in both Car powder and Car/Ga gel formulations. All samples exhibited distinct C–O stretching vibrations at 1011 $cm^{-1}$ and C–H stretching vibrations at 2932 $cm^{-1}$.[12] Subsequently, thermogravimetric analysis (TGA) was conducted to evaluate the thermal stability of the synthesized materials, showing two distinct degradation phases (Fig. 2b). The initial weight loss (30–170 °C) was attributed to the evaporation of bound water, while the substantial mass reduction in the second phase (200–450 °C) corresponded to the decomposition of polysaccharide chains followed by subsequent carbonization.[13]

### 3.2. Biocompatibility testing

Biocompatibility serves as a critical evaluation criterion for biomedical materials in clinical applications, demanding exemplary performance to ensure long-term safety during interactions with host blood components, and cells. This study systematically assessed the biosafety profile of the biogel material through comprehensive hemocompatibility and cytocompatibility evaluations. First, the biogel underwent dynamic co-culture (37 °C, 1 h) with 5% rat whole blood *in vitro*. Macroscopic observation (Fig. 3a) revealed that all test groups (including Car, and Car/Ga) maintained transparent supernatants after biogel contact, contrasting sharply with the hemoglobin-dissolution-induced bright red supernatant in positive controls. Quantitative analysis through UV spectrophotometry ($\lambda = 545$ nm) demonstrated (Fig. 3b) that hemolysis rates across test groups remained within 2%, significantly

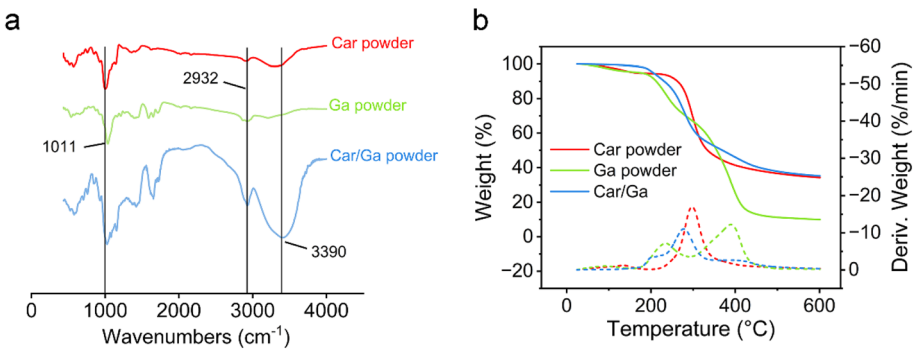


Fig. 2 (a) FTIR spectrum and (b) TGA curve of Car powder, Ga powder, and Car/Ga.

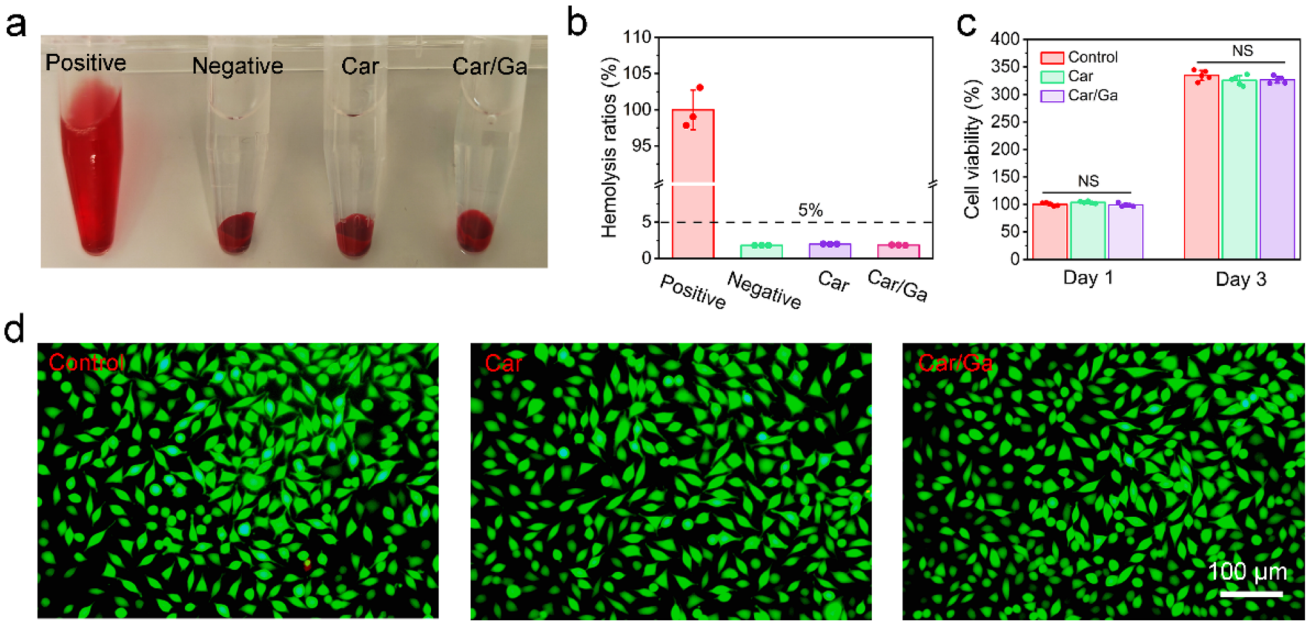


Fig. 3 (a) Photographs of rat blood after centrifugation and (b) hemolysis rate test after co-incubation with biogel ($n = 3$). (c) Survival rate of L929 cells after 1 day and 3 days of incubation with biogel ($n = 5$). (d) Live-dead staining photos of cells after 3 days of co-incubation with biogel.

below the 5% safety threshold mandated by ASTM F756 standard.[14]

Cytocompatibility assessment was then performed. To precisely assess the cytocompatibility of the biogel, we employed a co-culturing approach with murine fibroblast cells (L929). The CCK-8 assay revealed comparable cellular proliferation rates between the biogel group and the control group after 1 day and 3 day incubation periods (Fig. 3c), with no statistically significant differences observed ($p > 0.05$). This quantitative analysis demonstrated that the biogel did not exert inhibitory effects on fibroblast growth during the experimental timeframe. Calcein-AM/PI dual-staining fluorescence imaging (Fig. 3d) revealed characteristic spindle morphology and homogeneous green fluorescence distribution (viable cells) in test groups, while red fluorescence (necrotic cells) remained undetectable. Viable cell proportion reached 99.2 ± 0.6%, showing no statistical difference from negative controls ($p > 0.05$). These multidimensional evaluations substantiate the biogel's excellent biosafety profile in blood component interactions and cellular responses, demonstrating neither hemolytic effects nor cytotoxic responses. The material fully complies with fundamental biological requirements for biomedicine applications.

### 3.3. Investigation of anti-swelling properties and mechanisms in Car/Ga

This study systematically investigated the swelling kinetics of Car and Car/Ga biogels in urine environments through *in vitro* swelling experiments. Specifically, standardized hydrogel specimens were fully immersed in fresh urine medium, with their mass variations continuously monitored using a precision electronic balance over 0–72 hours until swelling equilibrium was achieved. The swelling kinetic profiles depicted in Fig. 4a reveal analogous swelling patterns for both formulations: only negligible mass increases (<0.5%) were detected during the initial 24 hour period, primarily attributed to superficial urine adsorption through physical interactions. Notably, even after prolonged 72 hour immersion, the equilibrium swelling ratios for both hydrogels consistently remained below 1%, demonstrating their remarkably low swelling propensity in urinary conditions (Fig. 4b).

Subsequently, we conducted a systematic investigation into the effects of urine exposure on the mechanical properties of biogel specimens. Following 72 hour immersion in simulated urine solution at physiological temperature (37 °C), the samples were retrieved for comprehensive mechanical characterization using standardized compression testing protocols. Remarkably, the stress–strain curves obtained from urine-treated samples demonstrated nearly complete overlap with baseline measurements taken prior to immersion, with a small variation observed in the linear elastic region (Fig. 4c). Quantitative analysis revealed Young's modulus values of 142.6 ± 6.16 kPa for control samples *versus* 135 ± 6.3 kPa for urine-exposed specimens, confirming no statistically significant alteration in mechanical stiffness (Fig. 4d).

This study reveals that the ultra-low swelling characteristics and mechanical stability of Car and Car/Ga dual hydrogels in urine may originate from the following synergistic mechanisms: (1) dense double-helix networks impede urine permeation *via* steric hindrance, preventing critical osmotic permeation. (2) Sulfate-cation electrostatic shielding reduces swelling pressure, while β-1,3-glycosidic bonds establish molecular hydration barriers. (3) The dual-helix bundles undergo stress-induced reversible unwinding-reentanglement transitions, dissipating energy through inter-helical slippage while maintaining structural integrity *via* rigid β-helical backbones. Future

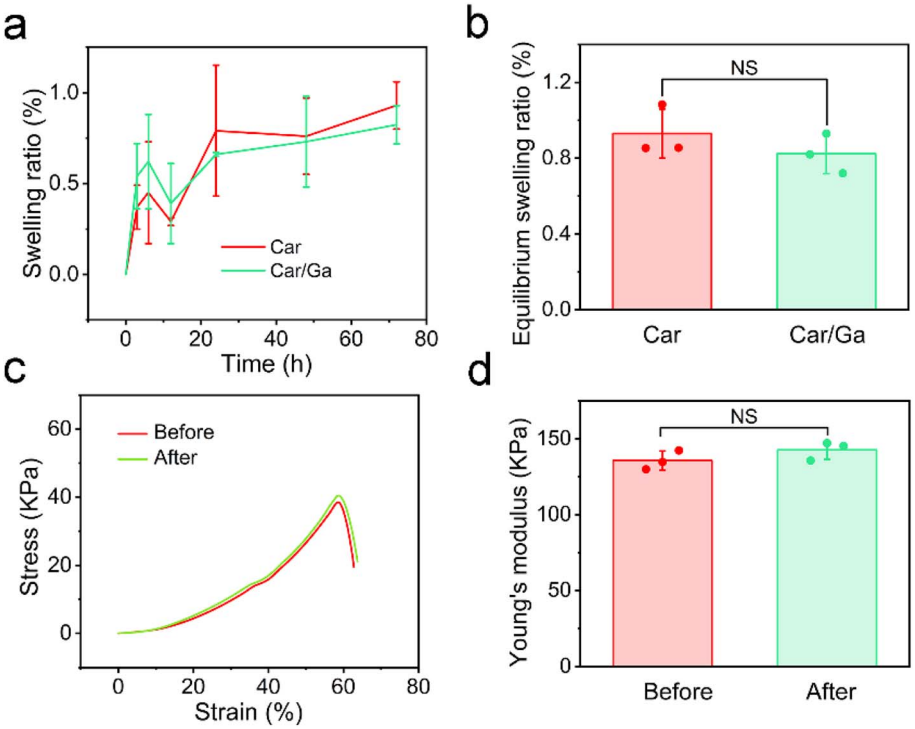


Fig. 4 (a) Swelling curves and (b) equilibrium swelling rates of Car and Car/Ga within 72 hours ($n = 3$). (c) Stress–strain curves and (d) Young's modulus of Car/Ga before and after immersion in urine ($n = 3$).

investigations should employ molecular dynamics simulations coupled with *in situ* characterization techniques to elucidate molecular interactions at the gel–urine interface.

### 3.4. Construction and treatment of trauma-induced urethral stricture

We developed a novel trauma-induced urethral stricture animal model replicating clinically relevant pathological features, establishing an experimental platform for evaluating the therapeutic efficacy of biogel *in vivo* (Fig. 5). One hour prior to the procedure, animals received prophylactic amoxicillin (50 mg $kg^{-1}$, intraperitoneal administration) for infection prevention. Under isoflurane inhalation anesthesia, subjects were positioned in dorsal recumbency. A ventral skin incision was made to expose the urethra, followed by precise insertion of a lubricated 0.03 inch diameter polyurethane guidewire into the

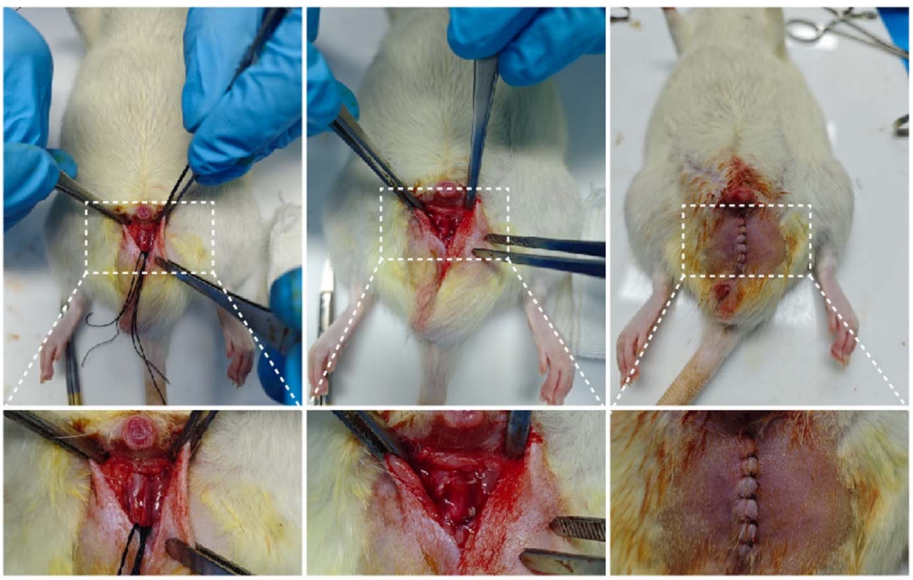

Fig. 5 Experimental protocol for establishing trauma-induced urethral stricture animal models and therapeutic application of biogel systems.

urethral lumen. Under direct visualization, a 5 mm full-thickness longitudinal incision was created along the guidewire trajectory, ensuring complete transection of all urethral wall layers until guidewire exposure was confirmed. The surgical site was subsequently filled with pre-synthesized biogel and closed using 5–0 PGA absorbable sutures with meticulous technique.

### 3.5. Imaging evaluation

Following intraurethral administration of iodinated contrast agent, radiographic imaging (Fig. 6) clearly delineated the anatomical architecture of the urethral lumen (red arrow) and bladder neck contour (blue arrow). Morphometric quantification revealed a characteristic contrast-filling defect approximately 1.0 cm distal to the external urethral orifice in control group animals, indicative of fibrotic stricture formation. In marked contrast, the Car/Ga treatment group exhibited significant reparative efficacy. Complete urethral continuity with intact contrast opacification was observed throughout the urethral course, demonstrating comparable luminal width at the injury site to that of normal urethral tissue.

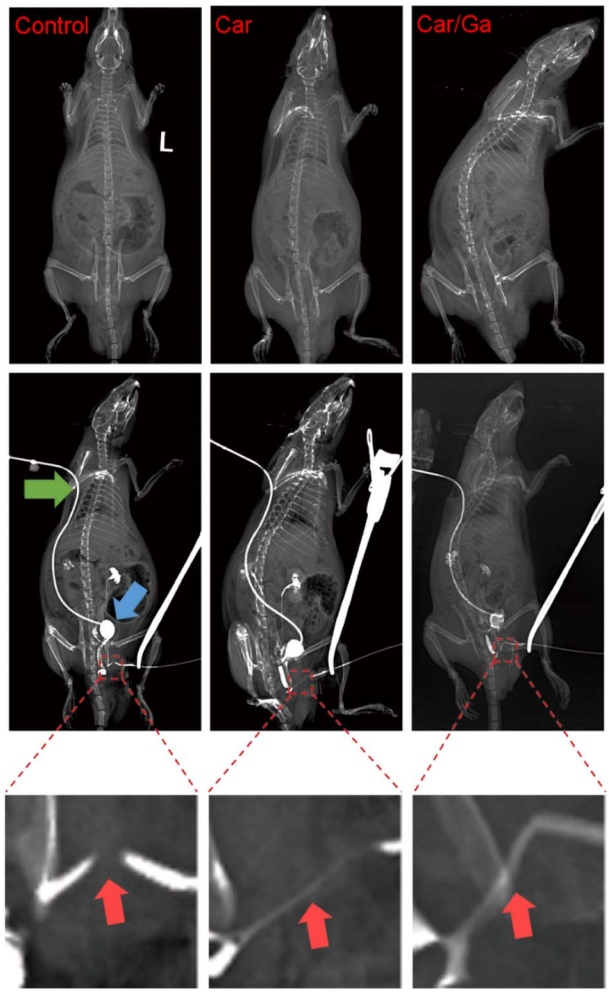


Fig. 6 Urethrography provides diagnostic imaging for localization and characterization of urethral injuries.

### 3.6. Anatomical evaluation

Four weeks postoperatively, gross anatomical examinations of the urethral tissues were conducted across all experimental groups (Fig. 7). The findings revealed that control group specimens demonstrated significantly increased scar tissue proliferation with marked urethral stricture occurrence. While all experimental groups exhibited mild scar formation, the extent was substantially reduced compared to control specimens. Notably, the Car/Ga treatment group displayed smooth tissue surfaces with superior regenerative outcomes, demonstrating exceptional therapeutic efficacy. The neoformed tissues achieved seamless integration with surrounding native tissues, showing no discernible boundaries at the repair sites.

### 3.7. Histopathological analysis

Histopathological analysis revealed distinct morphological differences between experimental groups. In control specimens, significant tissue architecture disruption was observed, characterized by pathological scar hyperplasia during the wound remodeling phase and subsequent development of secondary urethral stricture (Fig. 8a). In striking contrast, the Car/Ga-treated group exhibited well-organized epithelial basal tissue with loose yet continuous arrangement, demonstrating striking morphological resemblance to native urethral architecture. The therapeutic group displayed three characteristic histopathological improvements: (1) homogeneous collagen fiber distribution with well-aligned orientation patterns (Fig. 8b); (2) complete resolution of localized inflammatory cell infiltration; (3) quantitative analysis demonstrated comparable collagen layer thickness to healthy, providing critical structural evidence for tissue regeneration (Fig. 8c). These collective findings substantiate the treatment's capacity to restore physiological urethral microstructure, consistent with previous reports on regenerative matrix remodeling.[15]

### 3.8. Macrophage polarization analysis

This study systematically characterized macrophage polarization dynamics using dual immunofluorescence labeling for M1 (iNOS) and M2 (Arg1) phenotypic markers. Experimental results demonstrated that the Car/Ga composite elicited the most pronounced suppression of iNOS expression coupled with substantial Arg1 upregulation among treatment groups (Fig. 9a and b). Strikingly, quantitative analysis revealed a 79.2% reduction in iNOS fluorescence intensity and a 76.1% enhancement in Arg1 signal compared to controls, with statistical significance confirmed across comparative cohorts (Fig. 9c and d). Mechanistically, the composite orchestrates macrophage polarization through dual regulatory actions: selective inhibition of pro-inflammatory M1 activation and concurrent amplification of tissue-reparative M2 subpopulations. This precision immunomodulatory reprogramming effectively remodeled the immune microenvironment at urethral injury sites, attenuating fibrosis progression while alleviating the occurrence of urethral stricture.

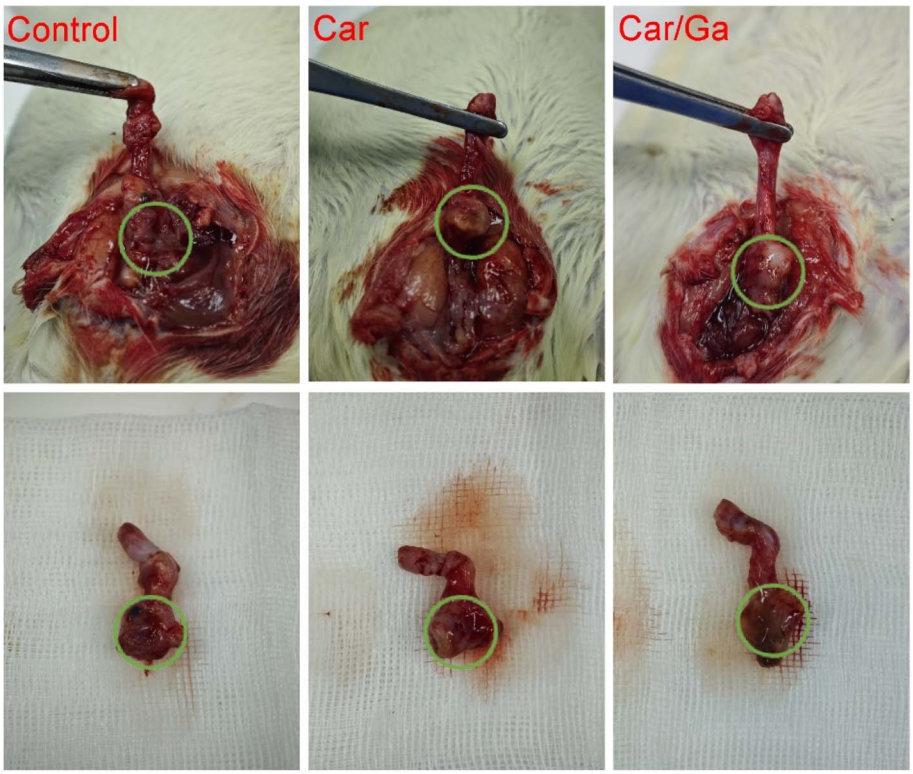


Fig. 7 The urethral specimens of all rats were harvested and representative photomicrographs were obtained following the 4 week experimental period.

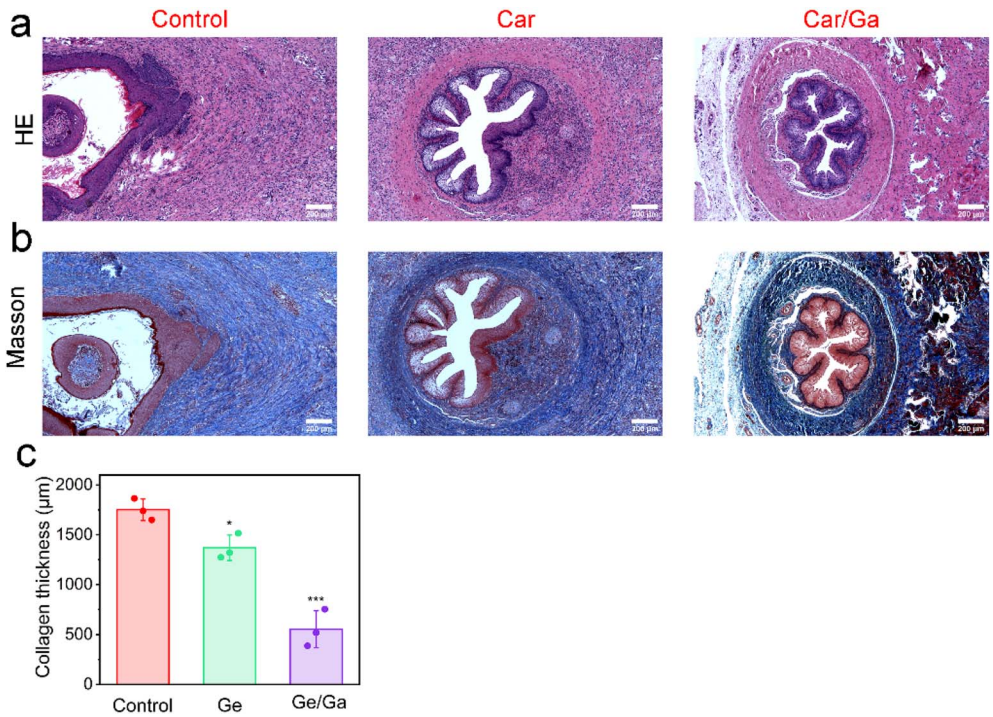


Fig. 8 Following the experimental period, the urethral wound tissues in rats were sectioned and stained with (a) HE and (b) Masson's trichrome for microscopic examination. (c) Comparative analysis of collagen thickness across experimental groups ($n = 3$).

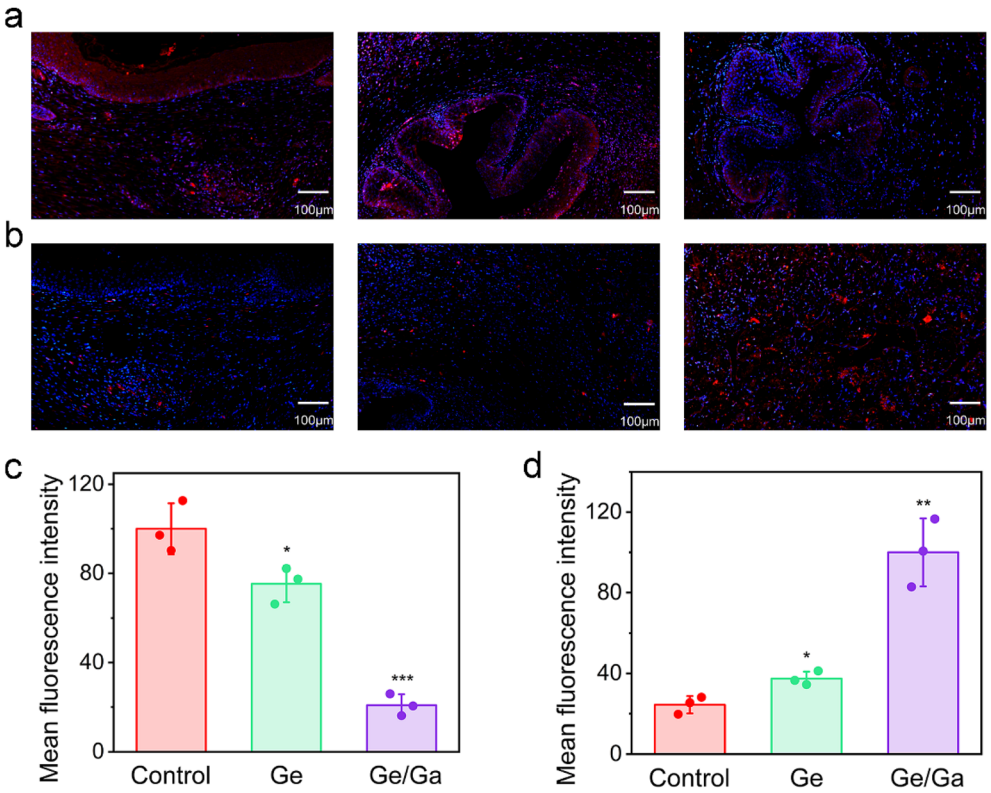


Fig. 9 Four weeks post-injury, immunofluorescence staining for (a) iNOS and (b) Arg-1 was performed on the urethral injury sites to investigate macrophage polarization. Statistical quantification of the average fluorescence intensity levels of (c) iNOS and (d) Arg-1 in the urethral wound area ($n = 3$).

### 3.9. Discussion on clinical applicability considerations

The Car/Ga biogel scaffold shows unique clinical advantages for traumatic urethral stricture repair by addressing structural instability and inflammatory microenvironments. Its anti-swelling carrageenan matrix maintains <1% swelling over 72 hours in urine, preventing secondary obstruction risks, while Ga – mediated immunomodulation (79.2% reduction in iNOS, 76.1% increase in Arg1) interrupts the inflammation–fibrosis cycle with mechanical reliability. For clinical translation, three key challenges need resolving. First, biological barriers: Ga's long – term pharmacokinetics and off – target effects are unclear, requiring controlled release and tissue – specific targeting. Second, manufacturing scalability: carrageenan's thermosensitive gelation process needs quality control for batch – to – batch consistency and standardization of Ga dispersion. Third, regulatory compliance: comprehensive preclinical evaluations must address urethra – specific biocompatibility and long – term safety concerns need longitudinal toxicity studies. Future work should use large – animal models and comparative trials to make the Car/Ga system a precision therapeutic for urethral stricture management.

## 4. Conclusions

This study developed a Car/Ga biogel scaffold combining anti-swelling carrageenan and immunomodulatory glycyrrhizic acid for precise urethral stricture repair. The system synergistically addressed structural and immunological regeneration challenges: (1) Car/Ga biogel maintained <1% swelling over 72 hours with mechanical stability, preventing secondary obstruction risks common in conventional hydrogels. (2) Ga modulated trauma microenvironments, reducing M1 macrophage markers (79.2% iNOS decrease) while enhancing M2 phenotypes (76.1% Arg1 increase), breaking inflammation–fibrosis cycles. (3) *In vivo* results showed reduced scarring, improved epithelial regeneration, and restored urethral continuity through imaging/histology. (4) Biocompatibility tests confirmed safety (<2% hemolysis, 99.2% cell viability). By integrating microenvironment stabilization and immune regulation, Car/Ga overcomes both mechanical failures and fibrotic recurrence mechanisms in current biomaterials. These findings underscore the therapeutic potential of phytochemical-integrated biomaterials for complex tissue regeneration. Future work will optimize release dynamics and advance toward human trials.

## Data availability

All relevant data are within the paper.

## Conflicts of interest

There are no conflicts to declare.

## Acknowledgements

This work was supported by the National Natural Science Foundation of China (82303571 and 82300790), the Hunan Provincial Natural Science Foundation of China (2023JJ40912 and 2023JJ40905).

## References

1 K. Li, K. Ding, Q. Zhu, F. Han, X. He, S. Tan, Z. Wu, Z. Zheng, Z. Tang and Y. Liu, Extracellular matrix stiffness aggravates urethral stricture through Igfbp3/Smad pathway, *Sci. Rep.*, 2023, **13**(1), 14315.

2 Z. Wu, Z. Tang, Z. Zheng and S. Tan, A novel trauma induced urethral stricture in rat model, *Sci. Rep.*, 2024, **14**(1), 6325.

3 J. Tian, D. Fu, Y. Liu, Y. Guan, S. Miao, Y. Xue, K. Chen, S. Huang, Y. Zhang, L. Xue, T. Chong and P. Yang, Rectifying disorder of extracellular matrix to suppress urethral stricture by protein nanofilm-controlled drug delivery from urinary catheter, *Nat. Commun.*, 2023, **14**(1), 2816.

4 X. Qi, X. Ge, X. Chen, E. Cai, Y. Xiang, H. Xu, Y. Li, Y. Lan, Y. Shi, H. Deng and J. Shen, An Immunoregulation Hydrogel with Controlled Hyperthermia-Augmented Oxygenation and ROS Scavenging for Treating Diabetic Foot Ulcers, *Adv. Funct. Mater.*, 2024, DOI: **10.1002/adfm.202400489**.

5 X. Qi, X. Tong, S. You, R. Mao, E. Cai, W. Pan, C. Zhang, R. Hu and J. Shen, Mild Hyperthermia-Assisted ROS Scavenging Hydrogels Achieve Diabetic Wound Healing, *ACS Macro Lett.*, 2022, 861–867.

6 A. Bassam, M. Du, Y. Li and X. He, Engineering in NIR-responsive photothermal materials and their application in wound healing administration, *Res. Mater.*, 2025, **3**(1), e20240031.

7 Y. Hua, K. Wang, Y. Huo, Y. Zhuang, Y. Wang, W. Fang, Y. Sun, G. Zhou, Q. Fu, W. Cui and K. Zhang, Four-dimensional hydrogel dressing adaptable to the urethral microenvironment for scarless urethral reconstruction, *Nat. Commun.*, 2023, **14**(1), 7632.

8 Q. Zeng, N. Tang, G. Shi and M. Zhang, Biogel Library-Accelerated Discovery of All-Natural Bioelectronics, *ACS Sens.*, 2024, **9**(12), 6685–6697.

9 Y. Qian, Y. Zheng, J. Jin, X. Wu, K. Xu, M. Dai, Q. Niu, H. Zheng, X. He and J. Shen, Immunoregulation in Diabetic Wound Repair with a Photoenhanced Glycyrrhizic Acid Hydrogel Scaffold, *Adv. Mater.*, 2022, **34**(29), e2200521.

10 A. Akbari, H. Abbasi, M. Shafiee and H. Baniasadi, Synergistic adsorption of methylene blue with carrageenan/hydrochar-derived activated carbon hydrogel composites: Insights and optimization strategies, *Int. J. Biol. Macromol.*, 2024, **265**(Pt 1), 130750.

11 M. Nakipoglu, Y. Özkabadayı, S. Karahan and A. Tezcaner, Bilayer wound dressing composed of asymmetric polycaprolactone membrane and chitosan-carrageenan hydrogel incorporating storax balsam, *Int. J. Biol. Macromol.*, 2024, **254**(Pt 3), 128020.

12 Y. K. Tao, Y. W. Tseng, K. Y. Tzou, C. Y. Kuo, H. T. Nguyen, H. T. Lu and A. E. Chuang, Advancing teeth whitening efficacy via dual-phototherapeutic strategy incorporating molybdenum disulfide embedded in carrageenan hydrogel for dental healthcare, *Int. J. Biol. Macromol.*, 2024, **276**(Pt 1), 133647.

13 X. Qi, W. Pan, X. Tong, T. Gao, Y. Xiang, S. You, R. Mao, J. Chi, R. Hu, W. Zhang, H. Deng and J. Shen, epsilon-Polylysine-stabilized agarose/polydopamine hydrogel dressings with robust photothermal property for wound healing, *Carbohydr. Polym.*, 2021, **264**, 118046.

14 N. Patiyananuwat, M. Safarzadeh, T. Chartpitak, K. Riansuwan, W. Ritshima and N. Nasongkla, In vitro and in vivo evaluation of the layer-by-layer vancomycin with poly(ε-caprolactone) nanosphere-coated Schanz pins for prolonged release, *J. Drug Delivery Sci. Technol.*, 2024, **100**, DOI: **10.1016/j.jddst.2024.106029**.

15 M. Yang, Y. Zhang, C. Fang, L. Song, Y. Wang, L. Lu, R. Yang, Z. Bu, X. Liang, K. Zhang and Q. Fu, Urine-Microenvironment-Initiated Composite Hydrogel Patch Reconfiguration Propels Scarless Memory Repair and Reinvigoration of the Urethra, *Adv. Mater.*, 2022, **34**(14), e2109522.